Bioorganic & Medicinal Chemistry Letters 22 (2012) 666–678

Contents lists available at SciVerse ScienceDirect

Bioorganic & Medicinal Chemistry Letters

journal homepage: www.elsevier.com/locate/bmcl

Synthesis, antitubercular evaluation and 3D-QSAR study of *N*-phenyl-3-(4-fluorophenyl)-4-substituted pyrazole derivatives

R.C. Khunt [a], V.M. Khedkar [b], R.S. Chawda [a], N.A. Chauhan [a], A.R. Parikh [a], E.C. Coutinho [b,*]

[a] *Department of Chemistry, Saurashtra University, Rajkot, Gujarat, India*
[b] *Department of Pharmaceutical Chemistry, Bombay College of Pharmacy, Kalina, Santacruz (E), Mumbai 400 098, India*

ARTICLE INFO

Article history:
Received 15 July 2011
Revised 26 September 2011
Accepted 18 October 2011
Available online 30 October 2011

Keywords:
Mycobacterium tuberculosis
Antitubercular agents
CoMFA
CoMSIA
3D-QSAR
Pyrazole

ABSTRACT

As a part of our ongoing research to develop novel antitubercular agents, a series of *N*-phenyl-3-(4-fluorophenyl)-4-substituted pyrazoles have been synthesized and tested for antimycobacterial activity in vitro against *Mycobacterium tuberculosis H37Rv* strain using the BACTEC 460 radiometric system. A 3D-QSAR study based on CoMFA and CoMSIA was performed on these pyrazole derivatives to correlate their chemical structures with the observed activity against *M. tuberculosis*. The CoMFA model provided a significant correlation of steric and electrostatic fields with the biological activity while the CoMSIA model could additionally shed light on the role of hydrogen bonding and hydrophobic features. The important features identified in the 3D-QSAR models have been used to propose new molecules whose activities are predicted higher than the existing systems. This study provides valuable directions to our ongoing endeavor of rationally designing more potent antitubercular agents.

Tuberculosis (TB) is currently the leading killer of youth, women and patients suffering from AIDS. The duration of the present antitubercular therapy leads to patient non-compliance and this in turn has contributed to the development of drug resistance.[1] In recent years, the pandemic of AIDS poses a major impact on the worldwide spread of TB. However, since 1980s, the disease has seen resurgence due to a variety of changes in social, medical and economic factors. Concomitant with the resurgence of TB, is the appearance of multidrug-resistant TB which exposes the frailties of the current drug armamentarium.[2]

The chemistry of heterocyclic compounds has been an area of interest for the medicinal chemists working in the field of tuberculosis. A literature survey has revealed that pyrazole and their derivatives containing the N–N bond are active against many mycobacteria.[3–6] It has been reported that C_6-substituted pyrimidine derivatives display antitubercular activity and pyrazole derivatives possess significant anti-HIV activity. This fact motivated us to design chemical prototypes bearing these two moieties that would be active against both drug-resistant strains as well as against latent bacteria.[7–14]

In order to study and deduce the correlation between structure and biological activity of these *N*-phenyl-3-(4-fluorophenyl)-4-substituted pyrazole derivatives, Comparative Molecular Field Analysis (CoMFA)[15,16] and Comparative Molecular Similarity Analysis (CoMSIA)[17,18] studies were performed. The structure–activity relationship derived from these analyses was fruitfully utilized to design a set of novel pyrazole analogs whose activities are predicted to surpass those in the original set.

4-Formylpyrazole was synthesized by the Vilsmeier reaction which on Claisen condensation with substituted acetophenones yielded the chalcones. Further, the chalcones were converted to a

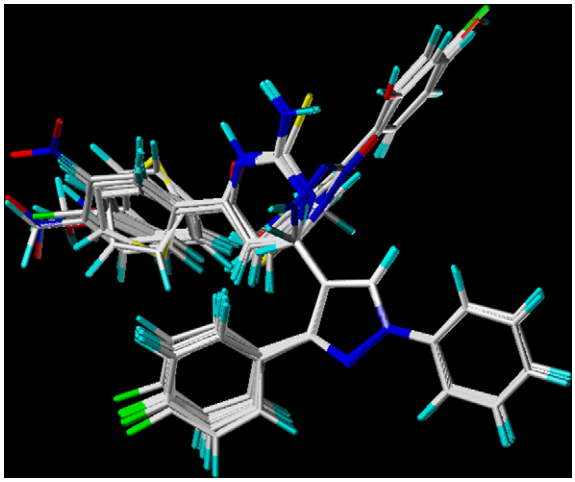

Figure 1. *Atom-fit alignment:* Training set aligned on minimum energy conformation of most active compound **11**.

* Corresponding author.
E-mail addresses: drrckhunt12@yahoo.com (R.C. Khunt), evans@bcpindia.org (E.C. Coutinho).

0960-894X/$ - see front matter © 2011 Elsevier Ltd. All rights reserved.
doi:10.1016/j.bmcl.2011.10.059

variety of *N*-phenyl-3-(4-fluorophenyl)pyrazole analogs by reaction with hydrazine hydrate. It must be noted here that the pyrazoline ring system has been constructed by nucleophilic cycloaddition of hydrazine hydrate with chalcones. The chalcones (**II**) are synthesised by the condensation of *N*-phenyl-3-(4-fluorophenyl)pyrazole-4-carboxaldehyde with aromatic ketones. This reaction produces a *cis* configuration of the double bond as judged by the coupling constant, J = 8.86 Hz, obtained in the NMR experiment. Due to the formation of *cis* isomer of chalcones (**II**), the nucleophilic addition of hydrazine results in the formation of the *R*-isomer of the pyrazoline (**III**) which was further confirmed by a plane polarised light experiment that showed right angle polarization. Nitroso and benzoyl groups were introduced at position-1 on the pyrazoline ring by treatment, respectively, with nitrous acid and benzoyl chloride. The chalcones (**II**) on condensation with thiourea and aminoguanidine gave 2-thio (**V**) or 2-amino-4-arylpyrimidines (**VI** and **VII**) (Scheme 1). The yields varied from 76% to 84% in case of chalcones (**II**); for the pyrazolines (**III**) the yields varied from 59% to 71% and from 51% to 69% for the pyrimidines (**VI**) and (**VII**). The structures of all compounds were confirmed by IR, ^{1}H and ^{13}C NMR and mass spectroscopy (refer to Supplementary data).

Antitubercular activity was determined using the modified BACTEC 460 system in which stock solutions as test molecules were prepared in dimethylsulfoxide (DMSO) at 1 mg/ml concentration and sterilized by passage through 0.22 μM PFTE filters.[19] All 51 compounds were tested for antitubercular activity against *M. tuberculosis H37Rv* strain. The concentrations required for 50% and 90% inhibition are given in Table 1 and these are in the range of 0.47–118.00 μM. Substitution of 1-(*p*-methoxyphenyl)-2-propen-1-one at the 4th position of the pyrazole ring produced the most active molecule (Compound **11**) with a IC_{50} of 0.47 μM (Table 1). It is interesting to note that for compound **46** with a 4-hydroxyphenyl-2-aminopyrimidine at position-4 of the pyrazole ring, concentrations of 0.88 and 0.47 μM are required for 90% and 50% inhibition, respectively. Thus, to understand the relationship between structure and activity, 3D-QSAR (CoMFA and CoMSIA) studies were carried out.

The 3D-QSAR studies (CoMFA and CoMSIA) were carried out with the QSAR module integrated in *Sybyl 7.1* (Tripos Inc., USA)[20] running on a Pentium IV computer under the Centos WS 4.8 as OS.

The CoMFA model generated with a training set of 33 *N*-phenyl-3-(4-fluorophenyl)-pyrazole analogs (carrying different pyrazoline and pyrimidine substituents at 4th position of pyrazole nucleus) is a six-component model with a cross-validated (leave-one-out)[21,22] correlation coefficient of 0.64 and standard error of 0.10. The non cross-validated Partial Least Squares (PLS)[23] analysis produced a model with regression coefficient (r^2) of 0.98 with *F*-test value of 175.52, indicating a good linear correlation between the observed and predicted activities for the molecules in the training set. The relative contribution of steric and electrostatic fields to the QSAR equation was found to be 43.3% and 56.7% respectively. External validation with the test set of 18 molecules yielded a predictive r^2 of 0.60, signifying the ability of the model to predict the activity of molecules beyond those used in its construction. An r^2 value of 0.98 obtained for 100 runs of bootstrap analysis[24] further supports the robustness and the statistical validity of the derived CoMFA model. The model was also tested for chance correlation by y-scrambling[25] (100 cycles) which yielded a poor r^2 of 0.18, thereby eliminating the possibility of chance correlation. The statistics of this CoMFA model generated are shown in (Table 2).

The same structural alignment and training/test sets as defined in the CoMFA studies were used to derive the CoMSIA models (Fig. 1). Several models were generated considering steric, electrostatic, hydrogen bonding and hydrophobic fields separately or in various combinations. With steric, electrostatic, H-bond donor and hydrophobic (SEDH) descriptor fields the CoMSIA model with 5 components produced a non cross-validated r^2 of 0.94, q^2 of 0.63, standard error of estimate 0.15, *F*-test value 190.49. The bootstrap r^2 of 0.97 obtained for 100 runs suggests a good internal consistency within the underlying dataset. Significantly low value of r^2,

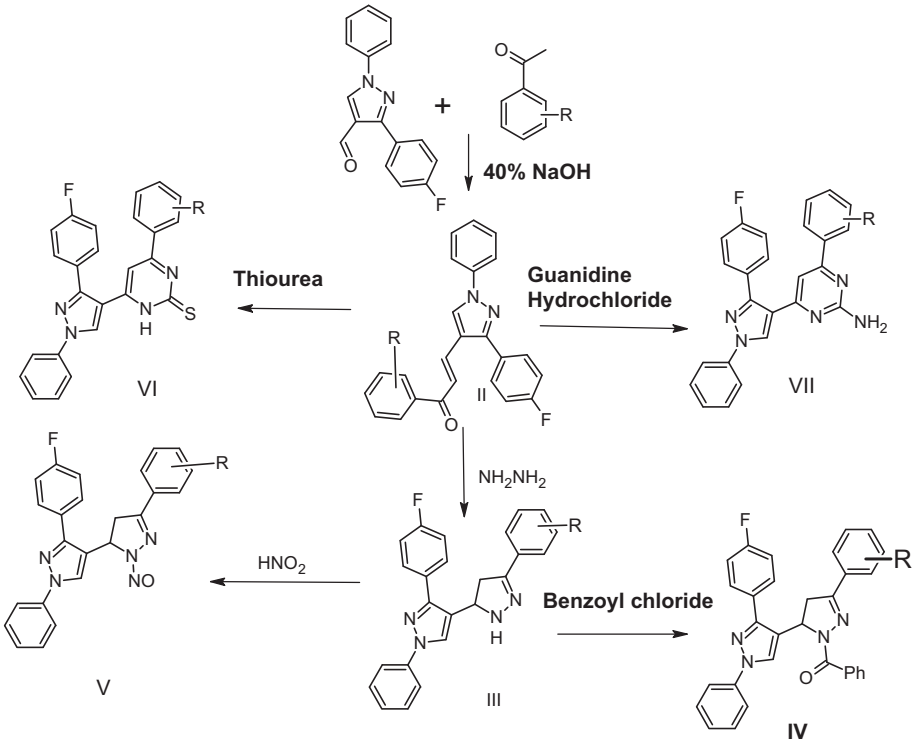

Scheme 1.

that is, 0.16 obtained with randomized activity (100 cycles) reveals that the model is stable and the results are not based on chance correlation. The relative contributions of the steric, electrostatic, hydrogen-bond donor and hydrophobic fields to this model are 27.3%, 15.3%, 15.7% and 41.6%, respectively. Further a predictive r^2 of 0.62 obtained for the test set compounds proved the predictive ability of the model. The statistics of this model are summarized in Table 2.

The other combinations viz (i) steric, electrostatic and hydrogen bond donor (SED), (ii) electrostatic, hydrophobic and hydrogen

Table 1
N-Phenyl-3-(4-fluorophenyl)-4-substituted pyrazole derivatives

Sr. No.	Structure	Melting point (°C)	Yield (%)	IC_{90} (μM)	IC_{50} (μM)	pIC_{90}	pIC_{50}
1	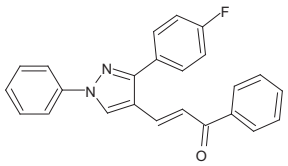	139–141	81	16.34	10.52	4.79	4.98
2	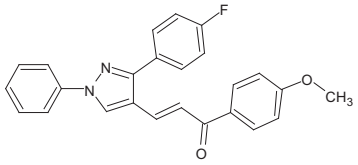	179–181	78	10.08	6.39	5.00	5.19
3	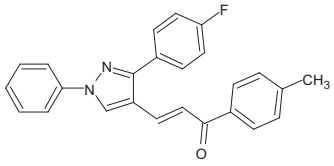	192–194	70	7.96	7.18	5.10	5.14
4	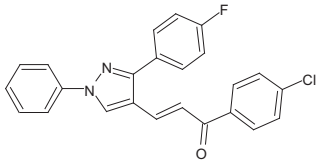	209–211	73	71.34	33.87	4.15	4.47
5	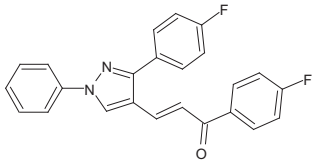	188–190	86	8.09	7.14	5.09	5.15
6	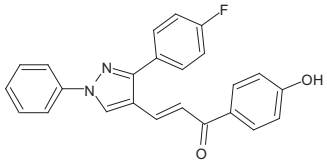	239–241	84	8.47	7.46	5.07	5.13
7	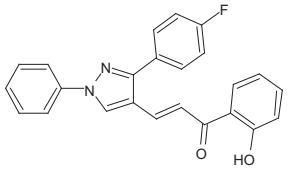	177–179	74	45.38	26.17	4.34	4.58
8	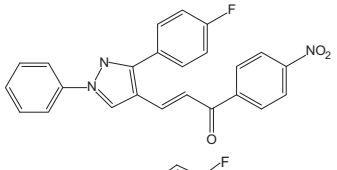	190–192	82	53.48	12.70	4.27	4.90
9	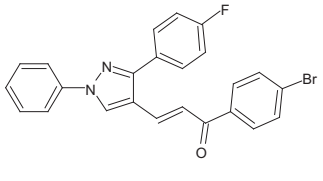	217–219	77	18.05	9.77	4.74	5.01

Table 1 (*continued*)

Sr. No.	Structure	Melting point (°C)	Yield (%)	IC_{90} (μM)	IC_{50} (μM)	pIC_{90}	pIC_{50}
10	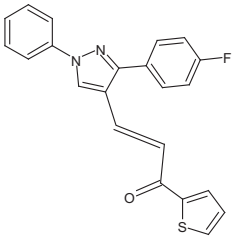	173–175	76	13.50	8.08	4.87	5.09
11	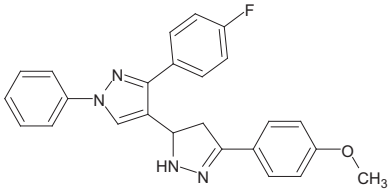	139–141	59	12.26	0.47	4.91	6.33
12	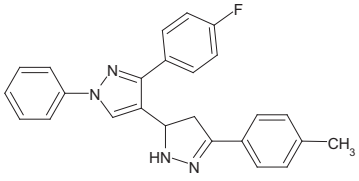	163–165	65	4.08	5.38	5.39	5.27
13	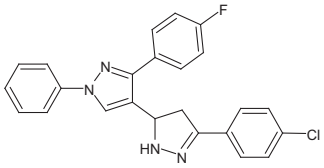	141–143	66	68.65	43.29	4.16	4.36
14	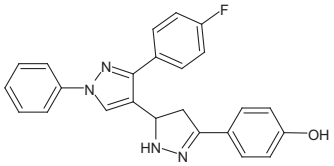	149–151	70	49.76	31.02	4.30	4.51
15	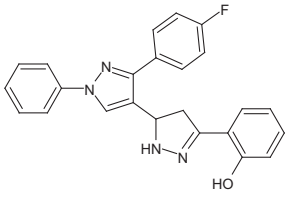	254–256	62	31.72	28.14	4.50	4.55
16	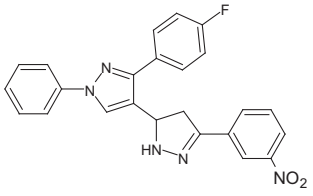	127–129	71	68.74	39.00	4.16	4.41
17	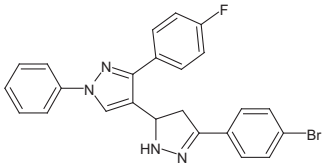	159–161	64	22.85	7.90	4.64	5.10
18	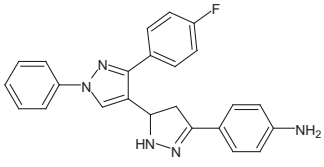	156–158	68	126.56	74.40	3.90	4.13

(*continued on next page*)

Table 1 (*continued*)

Sr. No.	Structure	Melting point (°C)	Yield (%)	IC_{90} (μM)	IC_{50} (μM)	pIC_{90}	pIC_{50}
19	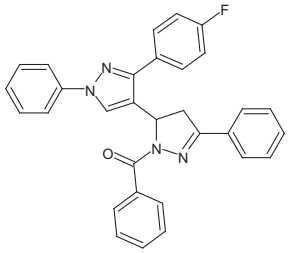	219–221	71	86.38	50.40	4.06	4.30
20	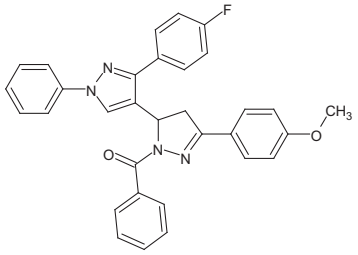	239–241	60	23.77	13.82	4.62	4.86
21	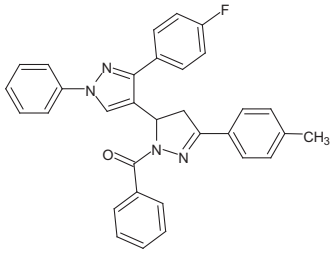	225–227	64	3.48	3.02	5.46	5.52
22	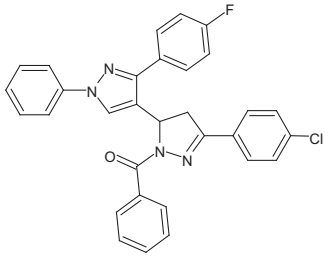	200–202	53	>191.94	51.42	<3.72	4.29
23	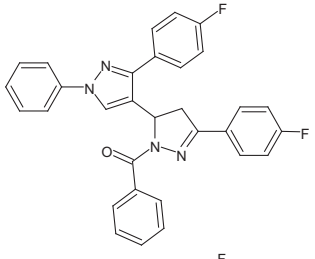	196–198	61	3.22	2.65	5.49	5.58
24	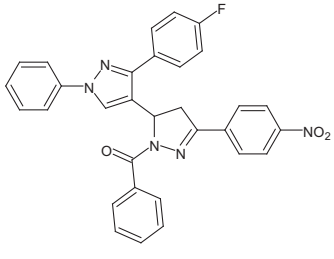	270–272	63	>187.42	57.43	<3.73	4.24

Table 1 (*continued*)

Sr. No.	Structure	Melting point (°C)	Yield (%)	IC_{90} (μM)	IC_{50} (μM)	pIC_{90}	pIC_{50}
25	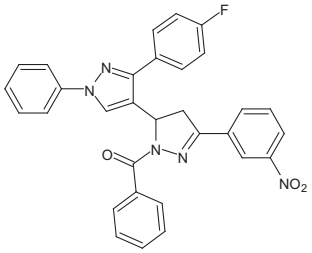	250–252	67	101.40	42.44	3.99	4.37
26	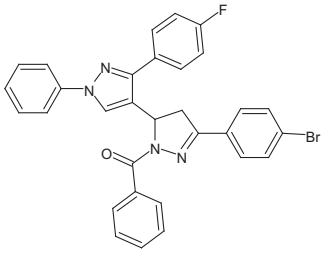	227–229	64	75.69	37.79	4.12	4.42
27	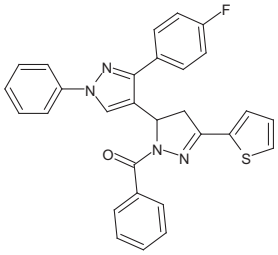	196–198	69	88.74	46.92	4.05	4.33
28	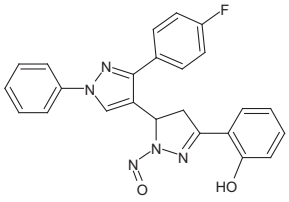	233–235	58	>233.96	118.80	<3.63	3.93
29	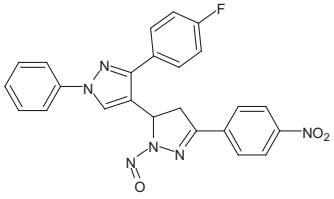	254–256	67	40.51	25.27	4.39	4.60
30	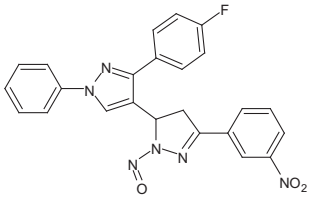	221–223	64	33.43	22.49	4.48	4.65
31	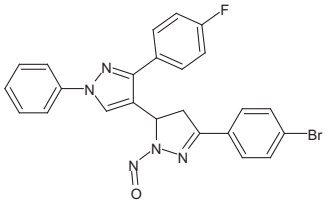	248–250	68	33.71	21.35	4.47	4.67

(*continued on next page*)

Table 1 (*continued*)

Sr. No.	Structure	Melting point (°C)	Yield (%)	IC_{90} (μM)	IC_{50} (μM)	pIC_{90}	pIC_{50}
32	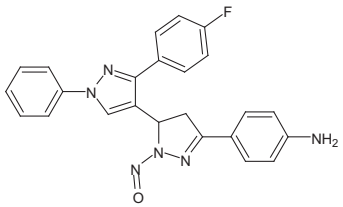	254–256	54	37.80	20.89	4.42	4.68
33	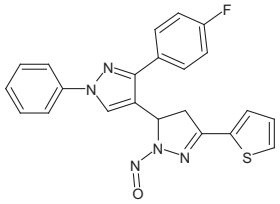	257–259	51	46.26	26.42	4.33	4.58
34	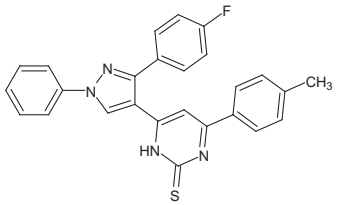	256–258	66	35.46	22.19	4.45	4.65
35	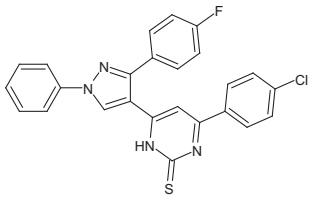	230–232	55	18.04	10.31	4.74	4.99
36	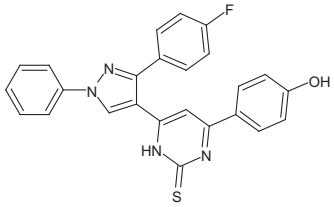	223–225	67	>227.02	69.24	<3.64	4.16
37	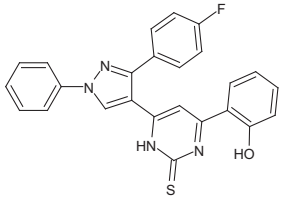	221–223	69	11.15	8.29	4.95	5.08
38	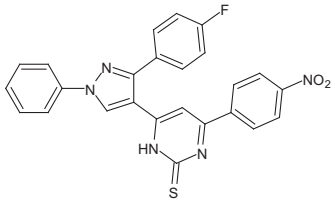	240–242	66	13.14	12.16	4.88	4.92
39	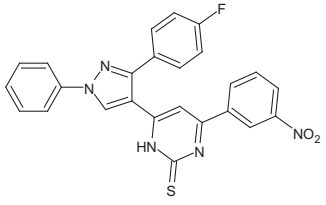	198–200	67	42.95	27.93	4.37	4.55

Table 1 (*continued*)

Sr. No.	Structure	Melting point (°C)	Yield (%)	IC_{90} (μM)	IC_{50} (μM)	pIC_{90}	pIC_{50}
40	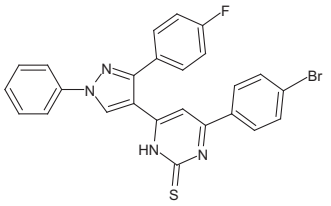	177–179	52	38.36	114.19	4.42	3.94
41	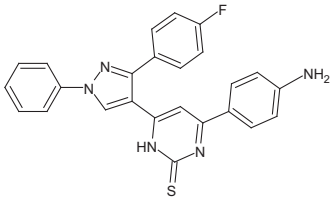	215–217	60	>227.53	22.09	<3.64	4.66
42	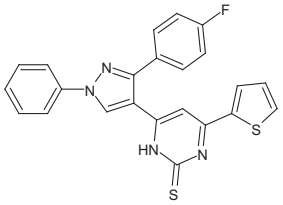	159–161	65	86.43	22.56	4.06	4.65
43	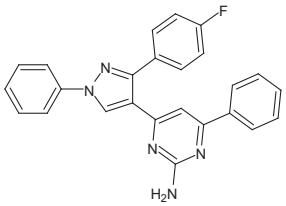	221–223	59	9.94	5.94	5.00	5.23
44	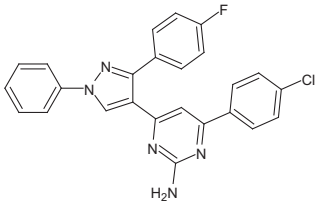	230–232	61	>226.30	95.47	<3.65	4.02
45	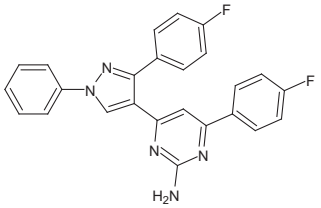	226–228	62	84.27	36.76	4.07	4.43
46	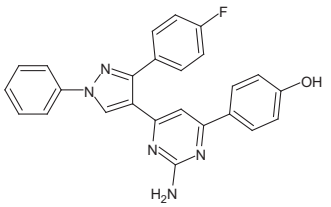	267–269	61	0.88	0.47	6.05	6.33
47	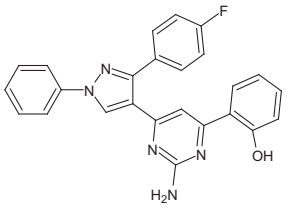	244–246	66	65.94	56.96	4.18	4.24

(*continued on next page*)

Table 1 (*continued*)

Sr. No.	Structure	Melting point (°C)	Yield (%)	IC_{90} (μM)	IC_{50} (μM)	pIC_{90}	pIC_{50}
48	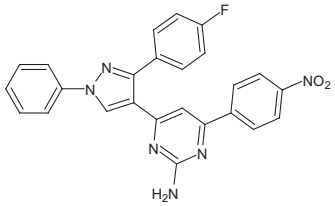	270–272	58	>220.04	75.36	<3.66	4.12
49	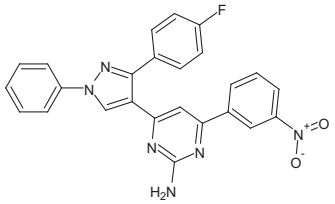	233–235	51	>220.04	52.92	<3.66	4.28
50	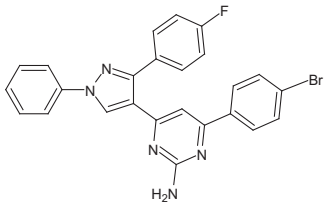	257–259	67	14.51	10.63	4.84	4.97
51	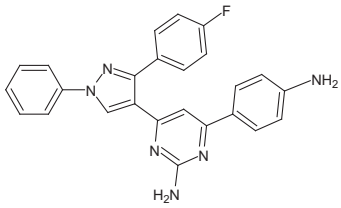	253–255	52	14.99	13.77	4.82	4.86

Table 2
Statistical results of the CoMFA and CoMSIA analyses

	CoMFA	CoMSIA (SEDH)
N	33	33
q^2	0.64	0.63
r^2	0.98	0.94
r^2_{pred}	0.60	0.62
r^2_{bs}	0.98	0.97
r^2 y-scrambling	0.18	0.16
F	175.52	190.49
SE	0.10	0.15
PLS components	6	5
Field contribution		
Steric	0.43	0.27
Electrostatic	0.57	0.15
H-bond donor	—	0.16
H-bond acceptor	—	—
Hydrophobic	—	0.42

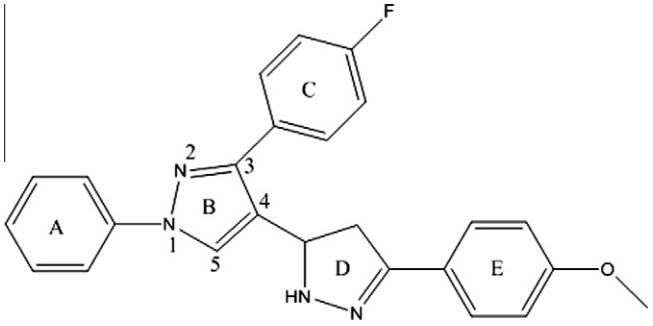

Figure 2. *N*-Phenyl-3-(*p*-fluorophenyl)-4-[3-(*p*-anisyl)-pyrazoline-5-yl]pyrazole (Compound **11**).

bond donor (EHD) and (iii) steric, electrostatic, hydrogen bond donor and acceptor (SEDA) in CoMSIA gave models with relatively low values for r^2 and r^2_{pred}.

The results of the CoMFA and CoMSIA studies can be visualized as 3D 'coefficient contour maps' contoured in terms of contribution. The most active compound **11** (Fig. 2) has been used to demonstrate the areas where a change in the molecular structure may affect its activity. The individual contributions of the favored and disfavored CoMFA/CoMSIA descriptor fields was fixed at 80% and 20%, respectively.

The CoMSIA steric and electrostatic contour maps were found to be in harmony with that of the CoMFA model and therefore for the sake of brevity only the CoMFA steric and electrostatic contours have been discussed. The CoMFA steric contour map (Fig. 3a) shows large green isopleths around the *para* position of the phenyl ring marked as (**E**) in Fig. 2. The steric contours suggest that bulky substituents could be added around this position to improve the potency. This is evident from the fact that molecules 2 (4-*methoxy*), **3** (4-*methyl*), **11** (4-*methoxy*) and **12** (4-*methoxy*) and **46** (4-*hydroxy*) show higher activity than compounds that lack a substituent at the *para* position of the phenyl ring (**E**). On the other hand, small yellow contours disfavoring steric bulk are also observed in the vicinity of the *ortho* and *meta* positions of the phenyl ring (**E**) suggesting that steric substituents at these positions would be detrimental for activity. This is substantiated by the fact that molecules **7** (2-*hydroxy*), **15** (2-*hydroxy*), **16** (3-*nitro*), **28** (2-*hydroxy*),

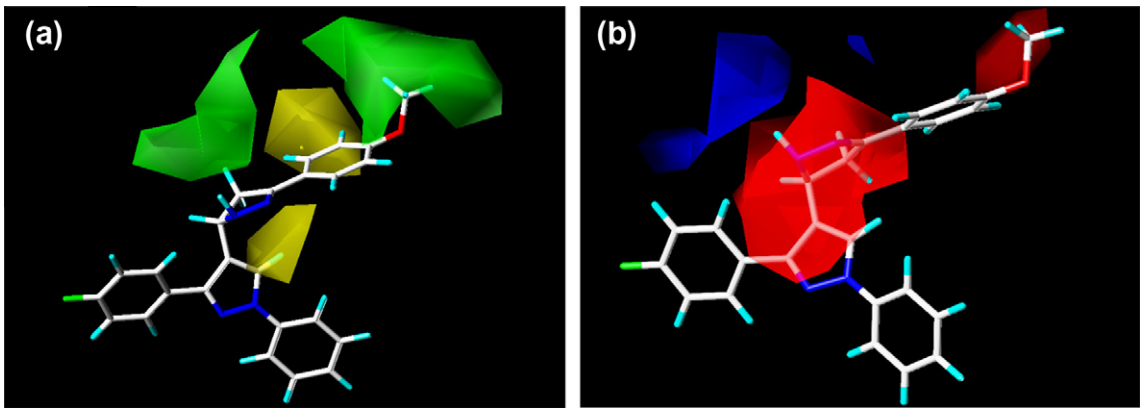

Figure 3. The CoMFA molecular interaction fields around Compound **11** (a) steric contours—green contours indicate regions where bulky groups increase activity, whereas yellow contours indicate regions where bulky groups decrease activity (b) electrostatic contours—red contour indicate regions where negative groups increase activity, whereas blue contours indicate regions where negative charge decreases activity.

30 (3-*nitro*) and **49** (3-*nitro*) with substituents around the *ortho* and *meta* positions of the phenyl ring (**E**) have activity lower than compounds with a substitution at the *para* position. There is a balance as noted by the green (favored) and yellow (disfavored) contours for steric groups (Fig. 3a) over the 4,5-dihydropyrazole (**D**) ring. Steric groups are found to be disfavored (yellow contour) over the nitrogen atoms of ring **D**. This is justified from the fact that molecules **19, 20, 22, 24, 25, 26, 27, 28, 29, 30, 31, 32** and **33** carrying a substituent on the pyrazoline nitrogen have poor antitubercular activity. On the other hand, the steric groups, shown in green, are preferred over the rest of the 4,5-dihydropyrazole (**D**) ring. Substituents on molecules **4, 35, 37, 43** and **46** were found to extend into this green contour.

The electronegative contours are found to influence the 3D-QSAR model more than the electropositive counterpart (Fig. 3b). No significant contribution is observed for electropositive substitution but both CoMFA as well as CoMSIA models display large red contours on the pyrazole (**B**) as well as the 4,5-dihydropyrazole (**D**) ring, suggesting that electronegative substitutions on these rings could be beneficial for the activity. An additional red contour favoring electronegative substitution is observed in the vicinity of the *para* position of the phenyl ring (**E**). Molecules **2, 5, 6, 11, 23** and **46** carrying electronegative substituents at these positions were found to be more active over those lacking substitutions. Only a small blue contour favoring electropositive substitution is observed around the 4th and 5th positions of the dihydropyrazole ring (**D**).

As regards H-bonding, a major cyan isopleth is observed in the vicinity of the nitrogen atoms of the 4,5-dihydropyrazole (**D**) ring suggesting that hydrogen bond donor functionality at these positions would enhance the activity while purple isopleths disfavoring H-bond donor functionality are observed around the nitrogen atoms of pyrazole ring (**B**) (Fig. 4a).

The hydrophobic CoMSIA fields (Fig. 4b) shown in yellow, indicate that the substituents at the *para* position of phenyl ring (**E**) need to be hydrophobic in nature so as to enhance the activity. Molecules **2**, **11**, **12** and **46** show higher activities than compounds that lack a substituent at the *para* position of the phenyl ring (**E**). Another yellow contour was also seen over the phenyl ring C suggesting that this ring is important for the activity. On the other hand white contours were observed around the nitrogen atoms of the 4,5-dihydropyrazole (**D**) ring signifying that the substituents at these positions need to be hydrophilic.

The structural features identified in the QSAR analysis were strategically utilized in the design of novel molecules with improved activity. Modifications were made to the core *N*-phenyl-3-(*p*-fluorophenyl)pyrazole structure as recommended by the CoMFA and CoMSIA isopleths. A few new molecules along with their predicted activities are given in Table 3. It is noteworthy that the activities of these new molecules are higher than most of the molecules in the training set. This indicates that the 3D-QSAR models presented here are powerful enough to suggest improvement in the poorly active molecules.

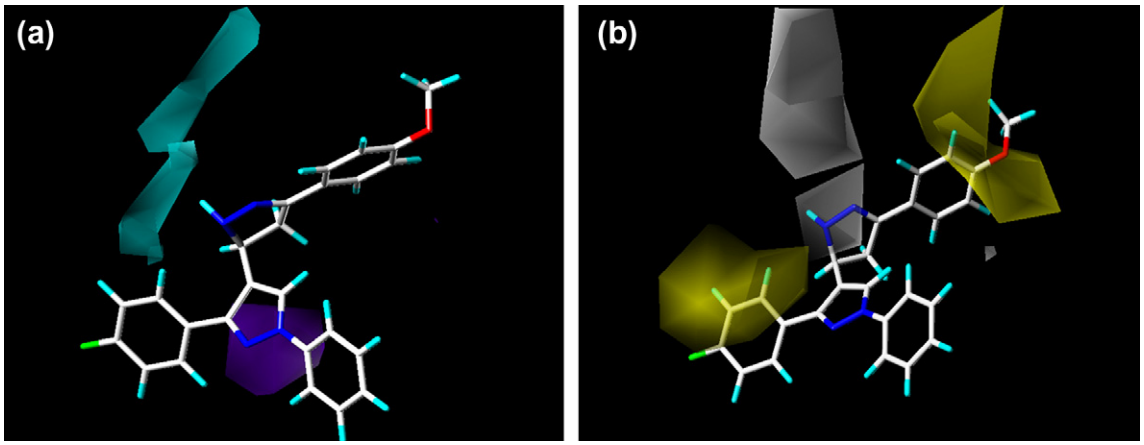

Figure 4. The CoMSIA molecular interaction fields around Compound **11**: (a) hydrogen bond donor contours—cyan contours indicate regions where H-bond donor group increases activity, whereas purple contours indicate regions where H-bond donor group decreases activity. (b) hydrophobic contour plots-yellow contours indicate regions where hydrophobic groups increases activity, whereas white contours indicate regions where hydrophobic group decreases activity.

In silico ADME and toxicity profiles were built for the *N*-phenyl-3-(*p*-fluorophenyl)-4-substituted pyrazole analogs with an objective to gain an insight into their pharmacokinetic and toxicity attributes. This was done with the *ADME/Tox web-box v3.5*[26,27] tool available

Table 3
Some antitubercular molecules designed with CoMFA and CoMSIA models with their predicted activities

Molecule	Chemical structure	Predicted activity (pIC_{50})
PYR01	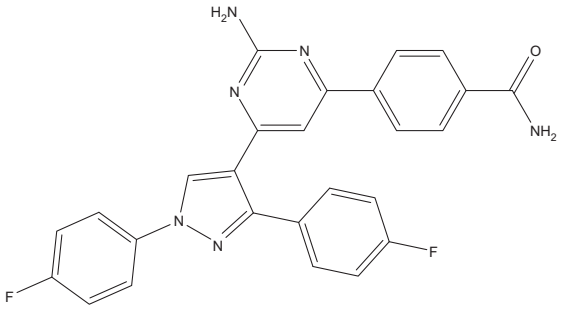	6.66
PYR02	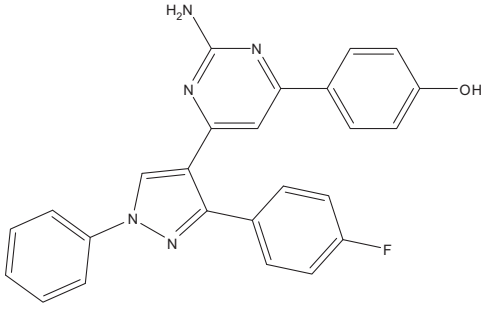	6.15
PYR03	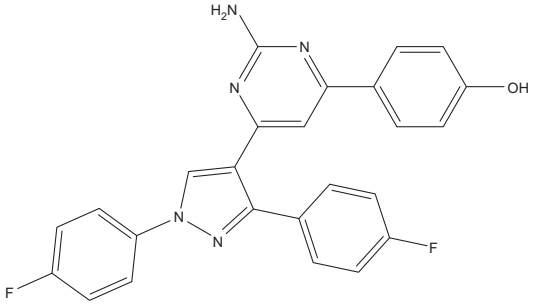	6.22
PYR04	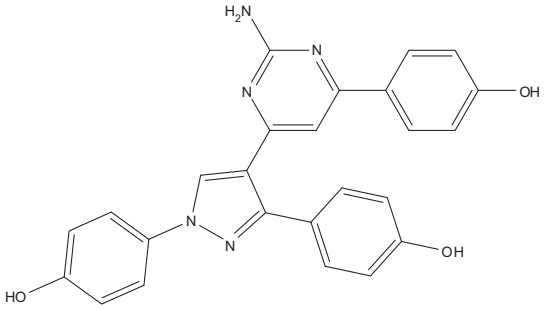	6.06
PYR05	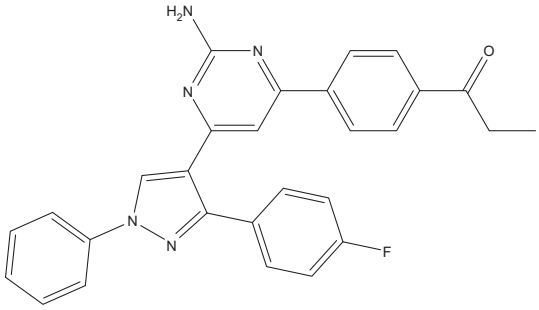	6.64

Table 3 (*continued*)

Molecule	Chemical structure	Predicted activity (pIC_{50})
PYR06	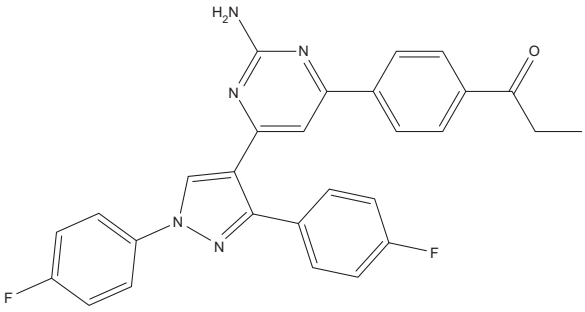	6.71
PYR07	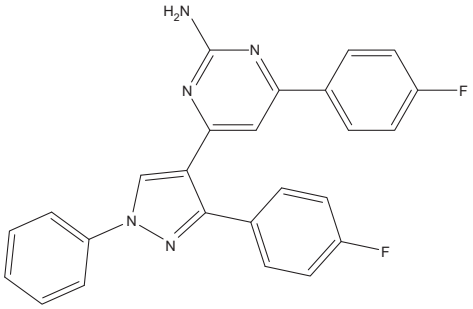	6.15
PYR08	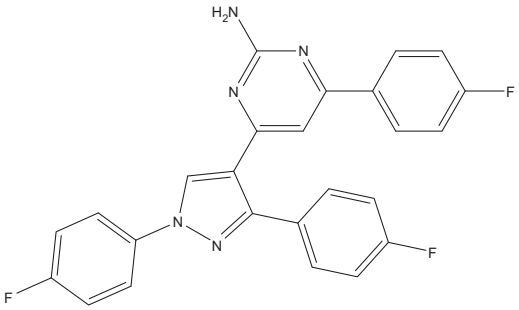	6.21

online. The ADME and toxicity profiles are given in the Supplementary data. Most of the molecules have a pK_a for the basic group in the range of 1.0–5.0 indicating that the pyrazole ring is weakly basic; for the acidic group it is around 9.0 suggesting that the hydroxyl group is weakly acidic. The average plasma protein binding for these molecules is around 94–99%. These molecules will predominantly bind to alpha1-acid glycoprotein and albumin. The molecules also display fairly good oral bioavailability with very low susceptibility to acid hydrolysis in the stomach. As *ADME/Tox web-box v3.5* does not predict clearance values, the bioavailability profile may have been derived only from the solubility and permeability of the molecules. Initial perusal of this data indicates that for most of these molecules the log*D* and log*P* values suggest moderate aqueous solubility. Toxicity predictions depict a high oral as well as iv LD_{50} dose, signifying that the molecules have a good safety margin. Also, these molecules show a low potential for genotoxicity as depicted by the low scores observed for the Ames test, except for molecules 28–33 for which the Ames score is predicted to be higher. Overall, the predicted pharmacokinetic and toxicity profiles for these molecules appear to be favorable for future lead optimization.

Conclusion

The synthesis and biological evaluation of a series of *N*-phenyl-3-(*p*-fluorophenyl)-4-substituted pyrazole derivatives as antitubercular agents has been discussed. Most importantly, this work validated our initial proposition that use of a pyrazole and pyrimidine substituted pyrazole scaffold would lead to molecules with potent antitubercular activity. The IC_{50} values for these compounds ranged from 0.47 to 118.0 μM. 3D-QSAR analysis was performed to rationalize the activity data for these pyrazole analogs. The CoMFA and CoMSIA models developed in this study have good predictive ability and can be useful in elucidating the relationship between the structures and their biological activities. The CoMFA and CoMSIA models are able to shed light on the role of steric, electrostatic, and hydrophobic fields around the molecules that can be strategically altered to modulate the antitubercular activity for these molecules. The pharmacokinetic and toxicity predictions for these pyrazole analogs provides additional information on their metabolic stability and safety profile which served as a guide to design new candidates with higher antitubercular activity.

Acknowledgements

Dr. R.C.K. thanks Saurashtra University for infrastructure facilities and DST, New Delhi for financial support under the Fast Track Young Scientist Scheme. V.M.K. thanks the Lady Tata Memorial Trust for the financial support. We also thank Dr. Cecil Kwong, TAACF, USA, for the antitubercular screening. The computational facilities were jointly provided by the All India Council of Technical Education through grant (F. No. 8022/RID/NPROJ/RPS-5/2003-04), the Department of Science and Technology through their FIST

program (SR/FST/LSI-163/2003), Department of Biotechnology (BT/PR11810/BRB/10/690/2009) and the Council of Scientific and Industrial Research (01/23/99/10-EMR-II).

Supplementary data

Supplementary data associated with this article can be found, in the online version, at doi:10.1016/j.bmcl.2011.10.059.

References and notes

1. Swaminathan, S. *Indian J. Pediatr.* **2002**, *69*, 44.
2. Rattan, A.; Kalia, A.; Ahmad, N. *Emerg. Infect. Dis.* **1998**, *4*, 195.
3. Kucukguzel, S. G.; Oruc, E. E.; Rollas, S.; Sahin, F.; Ozbek, A. *Eur. J. Med. Chem.* **2002**, *37*, 197.
4. Kucukguzel, S. G.; Rollas, S. *Farmaco* **2002**, *57*, 583.
5. Ali, M. A.; Yar, M. S. *Acta. Pol. Pharm.* **2007**, *64*, 139.
6. Ali, M. A.; Yar, M. S. *J. Enzyme Inhib. Med. Chem.* **2007**, *22*, 183.
7. Frieden, T. R.; Sterling, T. R.; Munsiff, S. S.; Watt, C. J.; Dye, C. *Lancet* **2003**, *362*, 887.
8. Maddry, J. A.; Suling, W. J.; Reynolds, R. C. *Res. Microbiol.* **1996**, *147*, 106.
9. Reynolds, R. C.; Bansal, N.; Rose, J.; Friedrich, J.; Suling, W. J.; Maddry, J. A. *Carbohydr. Res.* **1999**, *317*, 164.
10. Jones, P. B.; Parrish, N. M.; Houston, T. A.; Stapon, A.; Bansal, N. P.; Dick, J. D.; Townsend, C. A. *J. Med. Chem.* **2000**, *43*, 3304.
11. Pasqualoto, K. F.; Ferreira, E. I. *Curr. Drug Targets* **2001**, *2*, 427.
12. Teodori, E.; Dei, S.; Scapecchi, S.; Gualtieri, F. *Farmaco* **2002**, *57*, 385.
13. Vyas, R.; Udaibhan, G.; Verma, B. *Indian J. Heterocycl. Chem.* **2003**, *13*, 115.
14. El-Hashash, M.; Mahmoud, M.; Madboli, S. *Indian J. Chem.* **1993**, *32(B)*, 449.
15. Cramer, R. D., III; Patterson, D. E.; Bunce, J. D. *J. Am. Chem. Soc.* **1988**, *110*, 5959.
16. Cramer, R. D., 3rd; Patterson, D. E.; Bunce, J. D. *Prog. Clin. Biol. Res.* **1989**, *291*, 161.
17. Klebe, G.; Abraham, U.; Mietzner, T. *J. Med. Chem.* **1994**, *37*, 4130.
18. Klebe, G. *Perspect Drug Discovery Des.* **1998**, *12*, 87.
19. Collins, L.; Franzblau, S. G. *Antimicrob. Agents Chemother* **1997**, *41*, 1004.
20. Sybyl. Tripos Associates Inc.: 1699 S Hanley Rd., St. Louis, MO 631444, USA, 2005.
21. Stone, M. *J. Roy. Stat. Soc. B* **1974**, *36*, 111.
22. Richard, D.; Cramer, R. D., III; Bunce, J. D.; Patterson, D. E.; Frank, I. E. *Quant. Struct.-Act. Relat.* **1988**, *7*, 18.
23. Wold, S.; Johansson, E.; Cocchi, M. In *3D QSAR in Drug Design: Theory, Methods and Applications*; Kubinyi, H., Ed.; ESCOM Science Publishers: Leiden, 1993; p 523.
24. Shao, J. *J. Am. Stat. Assoc.* **1996**, *91*, 655.
25. Rucker, C.; Rucker, G.; Meringer, M. *J. Chem. Inf. Model.* **2007**, *47*, 2345.
26. Zmuidinavicius, D.; Japertas, P.; Petrauskas, A.; Didziapetris, R. *Curr. Top. Med. Chem.* **2003**, *3*, 1301.
27. Didziapetris, R.; Reynolds, D. P.; Japertas, P.; Zmuidinavicius, D.; Petrauskas, A. *Curr. Comput-Aided Drug Des.* **2006**, *2*, 95.